Journal of Geophysical Research: Oceans

RESEARCH ARTICLE
10.1029/2017JC013307

Winter Water Formation in Coastal Polynyas of the Eastern Chukchi Shelf: Pacific and Atlantic Influences

Daisuke Hirano[1,2], Yasushi Fukamachi[1,2,3], Kay I. Ohshima[1,2], Eiji Watanabe[4], Andrew R. Mahoney[2,3,5], Hajo Eicken[3,6], Motoyo Itoh[4], Daisuke Simizu[1,7], Katsushi Iwamoto[7,8,9], Joshua Jones[5], Toru Takatsuka[1], Takashi Kikuchi[4], and Takeshi Tamura[7,10,11]

[1]Institute of Low Temperature Science, Hokkaido University, Sapporo, Japan, [2]Arctic Research Center, Hokkaido University, Sapporo, Japan, [3]Global Station for Arctic Research, Hokkaido University, Sapporo, Japan, [4]Japan Agency for Marine-Earth Science and Technology, Yokosuka, Japan, [5]Geophysical Institute, University of Alaska Fairbanks, Fairbanks, AK, USA, [6]International Arctic Research Center, University of Alaska Fairbanks, Fairbanks, AK, USA, [7]National Institute of Polar Research, Tachikawa, Japan, [8]City of Mombetsu, Mombetsu, Japan, [9]Graduate School of Fisheries Sciences, Hokkaido University, Hakodate, Japan, [10]Department of Polar Science, School of Multidisciplinary Sciences, The Graduate University for Advanced Studies, Tachikawa, Japan, [11]Antarctic Climate and Ecosystems Cooperative Research Centre, University of Tasmania, Hobart, Tasmania, Australia

Key Points:
- Chukchi polynya winter ice production lacks a trend and is related to interannual fluctuations in northeasterly winds over Barrow Canyon
- Interannual variability of Alaskan Coastal Winter Water (ACWW) properties is influenced by variability of northeasterly winds
- Properties of ACWW are strongly influenced by waters of both Pacific and Atlantic origins

Correspondence to:
D. Hirano,
hirano@lowtem.hokudai.ac.jp

Citation:
Hirano, D., Fukamachi, Y., Ohshima, K. I., Watanabe, E., Mahoney, A. R., Eicken, H., et al. (2018). Winter water formation in coastal polynyas of the eastern Chukchi shelf: Pacific and Atlantic influences. *Journal of Geophysical Research: Oceans*, *123*, 5688–5705. https://doi.org/10.1029/2017JC013307

Received 25 JUL 2017
Accepted 21 JUN 2018
Accepted article online 2 JUL 2018
Published online 17 AUG 2018

Abstract Water properties and formation processes of Alaskan Coastal Winter Water (ACWW) over the eastern Chukchi shelf along the Alaska coast, the so-called Barrow Canyon pathway, are examined using data from moorings, atmospheric reanalysis, satellite-derived sea-ice production (SIP), and a numerical tracer experiment. Along this pathway, Pacific Winter Water (PWW) can be modified to produce ACWW through SIP accompanied by production of cold, saline polynya water in the coastal polynyas, upwelling of warm Atlantic Water (AW), and mixing processes on the shelf. Three different types of ACWW are formed: (i) a mixture of AW and PWW, (ii) a mixture of AW and polynya water, and (iii) hypersaline polynya water. The northeasterly winds, correlated with the north-south atmospheric pressure gradient between Beaufort High and Aleutian Low, are common triggers of polynya SIP episodes and AW upwelling in the Barrow Coastal Polynya (BCP). Due to the dual impact of northeasterly winds, PWW modification processes in the BCP are more complicated than what occurs elsewhere in the Chukchi Polynya. The impact of AW upwelling on the ACWW formation is most prominent in the BCP, usually centered along the coast. All types of ACWW are thought to be basically transported westward or northwestward with the Chukchi slope current and/or Beaufort Gyre and finally contribute to maintenance of the lower halocline layer especially over the Chukchi Borderland, Northwind Ridge, and southern Canada Basin. Even in the Pacific sector of the Arctic Ocean, ACWW properties are strongly influenced by both Atlantic-origin and Pacific-origin waters.

1. Introduction

Pacific-origin water entering the Chukchi Sea through Bering Strait reaches the shelf break via three pathways associated with bathymetric features: Herald Canyon on the western Chukchi shelf (Woodgate, Aagaard, & Weingartner, 2005), Central Channel between Herald and Hanna Shoals (Weingartner et al., 2005), and Barrow Canyon on the eastern Chukchi shelf (Pickart et al., 2005; Weingartner et al., 1998, 2005; Figure 1). In this study, we focus on the Barrow Canyon pathway through which water of Pacific origin is exported from Barrow Canyon, after passage through Bering Strait, and northward flow along Alaska's Chukchi Sea coast. In Barrow Canyon, persistent northeastward flow intensifies in summer and slows down in winter (Aagaard & Roach, 1990; Itoh et al., 2013; Weingartner et al., 1998; Weingartner et al., 2005). Recently, Weingartner et al. (2017) constructed a 37-year hindcast of the mean daily transport at the head of Barrow Canyon, and they showed the annual net transport cycle that comprises down-canyon transport of ~0.45 Sv in summer (May–September), up-canyon transport of ~0.1 Sv in fall (October–December), and a little more than zero in winter (January–April). Table 1 summarizes water mass/type definitions used in this study. Properties of the Pacific-origin water in Barrow Canyon vary seasonally alternating between warm, relatively fresh Pacific Summer Water (PSW, $S < 32.5$) and cold, relatively saline Pacific Winter Water (PWW, $32.5 < S < 33.1$). Warm, saline Atlantic Water (AW, $S > 34.0$) is centered at 300–400 m water depths in the Canada Basin (e.g., Jackson et al., 2010), below ~200 m in the Beaufort slope (e.g.,

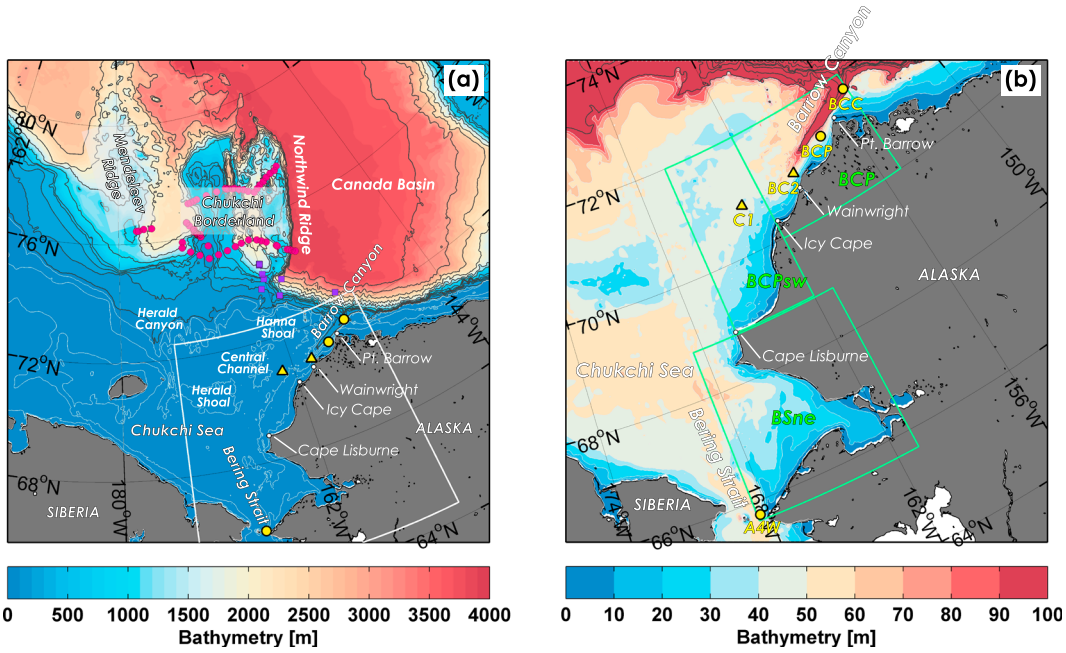

Figure 1. (a) Bathymetric map in the Pacific sector of the Arctic Ocean from the International Bathymetric Chart of Arctic Ocean (IBCAO version 3.0). The purple squares in the southern/southwestern Canada Basin and southeastern Chukchi Borderland areas represent the locations of hydrographic survey (Mirai2013 stations). The magenta circles in the Chukchi Borderland and Mendeleev Ridge areas indicate the locations of hydrographic survey (CBL2002 stations), where identified as the diapycnally ventilated region (Woodgate, Aagaard, Swift, et al., 2005). The enclosed region is shown in (b). (b) Detailed bathymetric map around the eastern Chukchi shelf. The yellow circles represent moorings mainly used in this study (A4W in the eastern Bering Strait, BCP in the Barrow Coastal Polynya, and BCC in Barrow Canyon). The yellow triangles represent additional moorings (C1 in Ladd et al., 2016 and BC2 in Weingartner et al., 2017). Coastal polynya areas along the Alaska Coast are defined as indicated by the green-enclosed regions labeled BCP, BCPsw, and BSne, respectively.

Nikolopoulos et al., 2009), and below ~150 m in Barrow Canyon (e.g., Itoh et al., 2013). From late fall to winter, prevailing northeasterly winds inhibit northeastward transport of PWW in Barrow Canyon and bring AW upwelling into Barrow Canyon (Aagaard & Roach, 1990; Woodgate, Aagaard, & Weingartner, 2005) and onto the eastern Chukchi shelf (Hirano et al., 2016; Ladd et al., 2016; Weingartner et al., 2017). In this way, Barrow Canyon is an important bathymetric feature as a gateway of Pacific-origin water into the Canada Basin and conversely of Atlantic-origin water onto the Chukchi shelf.

Table 1
Definitions of Water Masses and Types

Water mass and type		Salinity	Temperature (°C)	Remarks
Pacific Summer Water (PSW)		$S < 32.5$	$T > T_f + 1.0$	Hirano et al. (2016) after Itoh et al. (2013)
Pacific Winter Water (PWW)		$32.5 < S < 33.1$	$T < T_f + 1.0$	labeled "5" in Figure 11c, after Itoh et al. (2013)
Atlantic Water (AW)		$S > 34.0$	$T > 0.0$	labeled "6" in Figure 11c, after Itoh et al. (2013)
Polynya water		$33.1 < S < 34.0$	$T < T_f + 0.1$	labeled "4" in Figure 11c
Alaskan Coastal Winter Water (ACWW)	*type-1 (mixture of AW and PWW)	$S > 33.1$	lower halocline temperature $< T < 0.0$	labeled "1" in Figure 11c
	*type-2 (mixture of AW and polynya water)	$S > 33.1$–34.5	$T_f + 0.1 < T <$ lower halocline temperature	labeled "2" in Figure 11c
	type-3 (hypersaline polynya water)	$S > 34.0$	$T < T_f + 0.1$	labeled "3" in Figure 11c

*See details in section 2 and Figure 11c

Note. T_f is freezing point of seawater. In ACWW definitions, the "lower halocline temperature" serves as a measure rather than a unique temperature value; temperature warmer (colder) than the lower halocline temperature is presumably caused by more influence of warm Atlantic Water (cold Polynya Water) on their formation on the shelf (see details in section 6).

Polynyas are persistent and recurrent areas of open water and/or thin ice, where heat loss to the atmosphere is 1 or 2 orders of magnitude larger than that over thick ice (Maykut, 1978). Polynyas can be classified into two types: latent heat and sensible heat polynyas. The former is the result of divergent ice motion due to prevailing winds and/or ocean currents, whereas the latter is due to upward ocean heat flux (Melling et al., 2015; Morales Maqueda et al., 2004). Many Arctic polynyas are thought to be latent heat polynyas. In Arctic coastal polynyas over the shallow continental shelf, the whole water column likely reaches the freezing point (T_f) during cold seasons (Winsor & Björk, 2000), and therefore, heat loss is largely balanced by sea-ice production (SIP), which results in dense water formation through brine rejection. The Chukchi Polynya is the largest polynya in the western Arctic and forms in winter along the Alaska coast between Cape Lisburne and Point Barrow (Cavalieri & Martin, 1994; Itoh et al., 2012; Iwamoto et al., 2013, 2014; Tamura & Ohshima, 2011). Hirano et al. (2016) showed that the northernmost part of the Chukchi Polynya, which they named the Barrow Coastal Polynya (BCP), is a wind-driven hybrid latent and sensible heat coastal polynya.

The hybrid nature of the BCP results from the fact that the prevailing northeasterly winds are both parallel to Barrow Canyon and oblique to the coastline at Utqiaġvik (formerly known as Barrow). The latter condition results in an opening of the BCP by sea-ice divergence to promote SIP, while the former promotes upwelling of warm water into the BCP to inhibit ice growth (Hirano et al., 2016). A strong up-canyon shear flow established after the upwelling results in mixing events accompanied by ocean heat flux from the upwelled warm water into the surface layer, which played an important role in the formation and maintenance of the open water area (i.e., sensible heat polynya; Hirano et al., 2016). Such a characteristic sequence of promoting and suppressing SIP episodes in the BCP, both caused by the same northeasterly winds, is referred to as the BCP event. In the case of the 2009–10 ice growth season (November–May), five BCP events lasting from 4 to 17 days were identified, and ocean heat flux associated with the upwelled AW was estimated to be responsible for suppressing SIP in the BCP by 10–30% (Hirano et al., 2016). In addition, Ladd et al. (2016) observed five inflow events of upwelled AW during four winters of 2010/2011–2014/2015 (except for winter of 2012/2013) on the eastern Chukchi shelf off Icy Cape, ~225 km southwest from the head of Barrow Canyon (indicated by triangle labeled C1 in Figure 1b). They also suggested that the Chukchi Polynya is often classified as a hybrid polynya, based on their estimates of sufficient heat content in the upwelled AW to melt sea ice.

In this study, waters passing through Barrow Canyon (sea-ice growth season from November to May) are generically referred to as Alaskan Coastal Winter Water (ACWW), which is composed of PWW modified to varying degrees through modification processes earlier along the Barrow Canyon pathway. Salinity (hence density) of ACWW entering the Arctic basin depends on the original salinity of PWW at the Bering Strait and the amount of additional salt input associated with SIP along the pathway (Itoh et al., 2012; Winsor & Chapman, 2002). In the basin, ACWW intrudes into depths above the AW layer, because ACWW is lighter than AW. Thus, ACWW is one of the source waters to form and maintain the cold halocline layer and/or lower halocline layer that thermally insulates the cold, fresh surface mixed layer from the deep warm, saline AW (Aagaard et al., 1981; Rudels et al., 1996; Winsor & Björk, 2000). It is therefore likely that the modification processes of PWW along the Barrow Canyon pathway play a significant role in determining the properties of ACWW that actually enters the basin and also the depths at which such water ventilates. Due to the dual impact of northeasterly winds in both promoting and suppressing SIP in the BCP, we expect that the modification processes that PWW might experience around Barrow Canyon are more complicated than what occurs elsewhere in the Chukchi Polynya. Woodgate, Aagaard, Swift, et al. (2005) suggested that a lower halocline in much of the western Arctic was affected by the diapycnal ventilation, through the process that Atlantic-origin waters are upwelled onto the Chukchi shelf/slope to mix with Pacific-origin waters. Thus, understanding both Pacific and Atlantic influences is required to clarify the properties/formation processes of ACWW and also the upper ocean circulation in the western Arctic.

With a focus on variability in SIP and SIP suppression (indicative of the thermodynamic influence of AW upwelling) in the coastal polynyas, this study explores the difference in characteristics of BCP events observed under contrasting wind regimes (in terms of frequency/strength of the northeasterly winds) and the properties/formation processes of ACWW along the Barrow Canyon pathway. Based on these findings, this study discusses possible spreading paths of ACWW in the interior Arctic and an Atlantic-influence on the eastern Chukchi shelf in winter. Section 2 presents an overview of in situ observational data and a model experiment. Section 3 provides the climatology and variability of coastal polynyas along the Alaskan coast

Table 2
Detailed Information of the Moorings Deployed in the Barrow Coastal Polynya, Barrow Canyon, and the Bering Strait

	Mooring	Period	Location	Instrument	Sampling interval (min)	Nominal depth (m)	Bottom depth (m)
Barrow Coastal Polynya	BCP	30 July 2010 to 28 July 2011	71.24°N, 157.65°W	CT-Recorder (SBE37)	5	42	57
				ADCP (upward-looking) (RD Instruments WH-300)	20	51	
		11 August 2012 to 31 July 2013	71.20°N, 157.70°W	CT-Recorder (SBE37)	5	37	53
				ADCP (upward-looking) (RD Instruments WH-300)	15	41	
Barrow Canyon	BCC	11 September 2010 to 25 September 2012	71.73°N, 155.18°W	CTD (SBE37)	60	42, 81, 119, 179	283
				ADCP (upward-looking) (RD Instruments WH-300)	120	145	
				ADCP (downward-looking) (RD Instruments WH-300)	120	155	
		26 September 2012 to 5 September 2013	71.73°N, 155.19°W	CTD (SBE37)	60	44, 82, 121, 181	283
				ADCP (upward-looking) (RD Instruments WH-300)	120	146	
				ADCP (downward-looking) (RD Instruments WH-300)	120	156	
Bering Strait	A4W	1 August 2010 to 16 July 2011	65.76°N, 168.37°W	CTD (SBE16)	60	45	55
		10 July 2012 to 5 July 2013	65.76°N, 168.37°W	CTD (SBE16)	60	45	54

and the major factors controlling the variability of SIP in the BCP. Section 4 then presents the characteristics of BCP events observed in high and low SIP years. Sections 5 and 6 describe the water properties and formation processes of ACWW. Section 7 provides a discussion, and section 8 summarizes this study.

2. Data and Methods

2.1. In Situ Observation Data

As a collaborative study between Hokkaido University and University of Alaska Fairbanks, and a part of the Seasonal Ice Zone Observing Network, mooring observations have been continuously conducted within the BCP off Utqiaġvik, Alaska, on the northeastern Chukchi shelf since 2009 (circle labeled BCP in Figure 1b). The mooring configurations are similar to those shown in Hirano et al. (2016) (in their Figure 1c). Table 2 summarizes details of mooring data obtained in the BCP along with those obtained at the mouth of Barrow Canyon, and in the Bering Strait. To clarify the characteristics of BCP events for relatively low (2010–2011) and high (2012–2013) SIP years after 2009 (section 4), we use time series of temperature, salinity, and ocean current obtained by the BCP moorings for these two years (Fukamachi et al., 2011, updated 2014; Eicken et al., 2011, updated 2014). Although Hirano et al. (2016) flagged ocean current data when the Acoustic Doppler Current Profiler (ADCP) tilted over 20°, this situation generally occurred when strong up-canyon flows were set up during the BCP events. In order to seamlessly examine the characteristics of ocean currents during the BCP events, periods of flagged current data are interpolated using the following approach. First, we derive a regression for composite tilts and absolute velocities when the composite tilts derived from pitch and roll data are within the range of 10–20°. Second, the absolute velocities are interpolated by using the regression when the pitch or roll exceeds 20°, and current direction of the interpolated absolute velocity is set to an averaged direction for surrounding valid data (five data each before and after flagged periods). Finally, the Godin filter (Godin, 1972) was applied to the corrected ocean current data before resampling them every hour.

In Barrow Canyon, mooring observations have been continuously conducted by Japan Agency for Marine-Earth Science and Technology (JAMSTEC) since 2000. In order to examine the water properties of ACWW passing through Barrow Canyon (section 5), we use time series of temperature, salinity, and ocean currents measured at several depths at the center of Barrow Canyon (BCC) moorings in the central and deepest region of Barrow Canyon for 2010–2011 and 2012–2013 (Itoh et al., 2013; circle labeled BCC in Figure 1b). In the Bering Strait, mooring observations have been continuously conducted by University of Washington since 1990 (circle labeled A4W in Figure 1b). In order to examine PWW properties in Bering Strait (section 6),

we use time series of temperature and salinity measured at 10 m above the bottom of A4W moorings in the eastern part of the strait for 2010–2011 and 2012–2013 (Woodgate & Weingartner, 2015a, 2015b; Table 2).

In 2002, comprehensive hydrographic observations were conducted by *U.S. Coast Guard Cutter (USCGC) Polar Star* in the Chukchi Borderland (CBL) and Mendeleev Ridge area from late August to late September (Woodgate et al., 2002; magenta circles in Figure 1a, hereafter referred to as CBL2002 hydrographic data). In 2013, hydrographic observations were conducted in the southern/southwestern Canada Basin and southeastern CBL area by R/V *Mirai* in September (Nishino, 2013; purple squares in Figure 1a, hereafter referred to as Mirai2013 hydrographic data). We discuss where ACWW can contribute to ventilations after entering the basin, through comparison of water properties of the lower halocline in these regions and ACWW flowing into Barrow Canyon (sections 5 and 7.1).

2.2. Model Experiment

To visualize the upwelling of AW from the midlayer of the Canada Basin onto the Chukchi shelf, we also use the results from a tracer experiment for 2001–2014 using the Center for Climate System Research Ocean Component Model (COCO) version 4.9 (Hasumi, 2006). The pan-Arctic regional COCO model used in this analysis has reasonably reproduced major features of ocean circulation in the western Arctic (Hirano et al., 2016; Watanabe et al., 2014, 2015). The model configuration and experimental design are the same as those in the previous experiments (Watanabe et al., 2017). The sea-ice component is represented by one-layer thermodynamics (Bitz & Lipscomb, 1999) and elastic-viscous-plastic rheology (Hunke & Dukowicz, 1997) formulations. The ocean component is a free-surface general circulation model including the advection scheme of Leonard et al. (1994) and the mixed-layer turbulence closure scheme of Noh and Kim (1999). The model domain contains the entire Arctic Ocean, the Nordic seas, and the northern North Atlantic (see Figure 1b in Watanabe et al., 2017). The horizontal resolution is approximately 5 km, and there are 42 hybrid σ-z vertical levels. The vertical grid spacing varies from 2 m at the top level to 500 m at the deepest level.

For the tracer experiment, the model was integrated from January 2001 to December 2014. The atmospheric forcing components such as air temperature, specific humidity, downward radiative fluxes, and wind speed were obtained from the Climate Forecast System Reanalysis (CFSR: 1979–2010) and version 2 (CFSv2: 2011–2014) 6-hourly data set of the National Centers for Environmental Prediction (NCEP; Saha et al., 2010). At the Bering Strait, the idealized seasonal cycles of northward velocity, temperature, and salinity are prescribed to have an annual mean inflow of 0.8 Sv (1 Sv $\equiv 10^6$ m^3/s) and maximum temperature (salinity) in August (February). A virtual tracer with its concentration values of unity (indicating the pure, unmodified AW, hereafter referred to as the Atlantic-water tracer) is continuously released below 200 m depth in the whole model domain, and the tracer values for 0–200 m are reset to zero on 1 October every year. Advection and diffusion processes of the tracer are solved as well as temperature and salinity.

3. Climatology and Variability of SIP Along the Alaska Coast

3.1. Improved Estimates of SIP Rate Derived From Special Sensor Microwave Imager and Special Sensor Microwave Imager/Sounder Data

Iwamoto et al. (2014) estimated SIP rate in the Arctic using the Advanced Microwave Scanning Radiometer-Earth Observing System (AMSR-E) using a heat budget analysis with applying an open water mask (Iwamoto et al., 2013). According to Iwamoto et al. (2013), the open water mask can detect areas of open water (i.e., sensible heat polynyas) using PR_{89} values along the ice edge as a threshold to distinguish open water pixels from those of sea ice (PR_{89} is the polarization ratio [PR] of AMSR-E 89 GHz brightness temperatures). Due to high spatial resolution of AMSR-E (~6.25 km), the AMSR-E-derived SIP product can exclude small areas of open water and is suitable for analyzing variability of the hybrid BCP (Hirano et al., 2016). However, the AMSR data are available only after June 2002, with a 10-month data gap between the end of AMSR-E operation in September 2011 and the launch of AMSR2 in July 2012.

The Special Sensor Microwave Imager (SSM/I) and Special Sensor Microwave Imager/Sounder (SSMIS) have a spatial resolution (~12.5 km) only about one quarter in pixel density relative to AMSR-E, but SSM/I-SSMIS has the advantage of seamless data acquisition from 1992 to present. Using SSM/I-SSMIS data, Tamura and Ohshima (2011) provided the first mapping of SIP in the entire Arctic. In addition to their relatively coarse resolution, the SSM/I-SSMIS SIP data by Tamura and Ohshima (2011) were processed without applying the

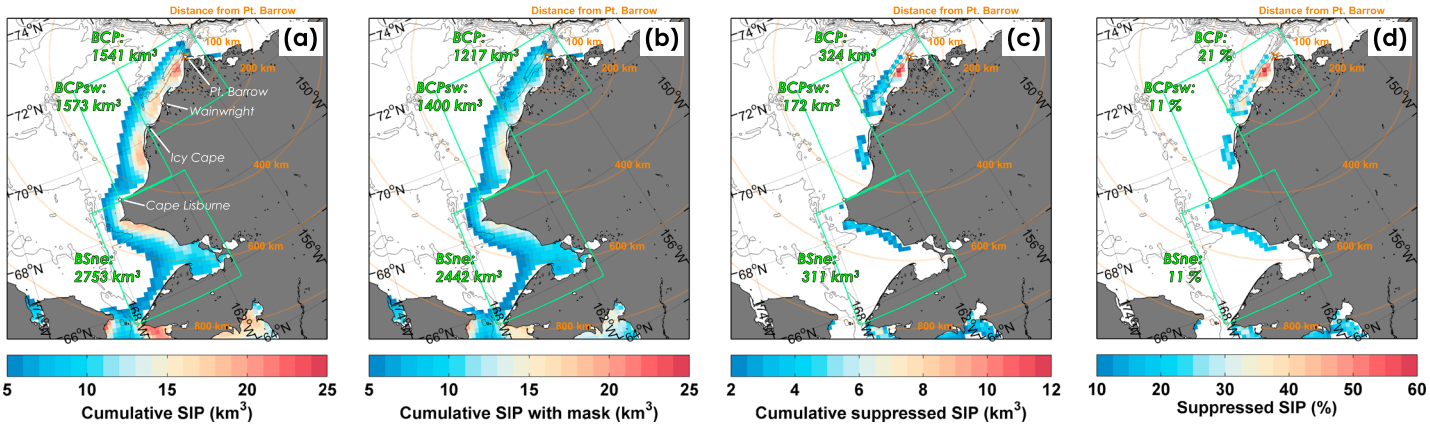

Figure 2. Climatology of Chukchi Polynya activity from November to May for 1992–2014. (a) Cumulative sea-ice production (SIP) without an open water mask (after Tamura & Ohshima, 2011). (b) Cumulative SIP with an open water mask (this study). (c) Difference between (a) and (b), that is, cumulative SIP suppression. (d) Fraction of SIP suppression. Total values for each polynya area are shown in all the panels.

algorithm with an open water mask implementation, such as adopted by Iwamoto et al. (2014). Therefore, the SSM/I-SSMIS SIP data tend to overestimate SIP rates, particularly in the BCP and possibly in the North Water Polynya, because the occurrence of sensible heat polynyas (open water area) in these areas is also affected by ocean heat.

To reveal long-term variability of SIP suppression caused by ocean heat flux (indicative of the thermodynamic influence of AW upwelling) in the hybrid BCP, the open water mask was also applied to the SSM/I-SSMIS algorithm of Tamura and Ohshima (2011), by adopting a method similar to that employed by Iwamoto et al. (2013) (in their Figure 8). $PR_{89} = 0.08$ (PR_{89} is the PR of SSM/I-SSMIS 89 GHz brightness temperatures) was adopted as a threshold to distinguish open water pixels from those of sea ice. On average, from November to May for 2002–2011, SSM/I-SSMIS-derived SIP rate when areas of open water are excluded over the BCP area (Figure 1b, see also section 3.2) is estimated to be ~38% (originally ~68% before applying the open water mask to the SSM/I-SSMIS data) higher than that derived from AMSR-E. However, SIP estimates derived from AMSR-E (Iwamoto et al., 2014) and SSM/I-SSMIS (Tamura & Ohshima, 2011) exhibit the similar tendencies during AMSR-E operation period for 2002–2011 (Figure 10 of Iwamoto et al., 2014). Therefore, our conclusions derived from SSM/I-SSMIS are essentially not different from those derived from AMSR-E. As suggested by Iwamoto et al. (2014), possible reasons for the difference between the SSM/I-SSMIS and AMSR-E SIPs are differences in spatial resolutions, no landfast ice detection mask in the SSM/I-SSMIS algorithm, and thinner bias of the SSM/I-SSMIS ice thickness. We successfully generate a longer, improved SSM/I-SSMIS SIP data set that takes into account the open water area in the entire Arctic for 1992–2014. The improved SIP estimates allow us to discuss climatology, trends, and long-term variabilities of SIP and SIP suppression.

3.2. Definition of Hybrid BCP Area Based on Climatology

Without using an open water mask, the climatological cumulative SIP from November to May for 1992–2014 derived from SSM/I-SSMIS data (Tamura & Ohshima, 2011) is characterized by high SIP along the Alaska coast (Figure 2a). When sensible heat polynyas, corresponding to areas of open water, are excluded by applying an open water mask, SIP is still highest near the coast, but is notably reduced, particularly in the northern region of the Chukchi Polynya (Figure 2b). Differences in SIP calculated with and without the open water mask (Figure 2c) are taken to be equivalent to the amount by which SIP is suppressed due to ocean heat flux. This SIP suppression is largest in the coastal region from Point Barrow to Icy Cape (within the northeastern green box in Figure 2). Especially for waters near Point Barrow subjected to the influence of upwelled AW from the Canada Basin via Barrow Canyon (Hirano et al., 2016), there is a marked SIP suppression of more than 10 km^3 in each grid cell for 22 years (Figure 2c), and the fraction of SIP suppression is estimated high at 40–60% (Figure 2d). Relatively high suppression of 10–30% is also found along the coast between Wainwright and Icy Cape (Figure 2d). Based on the spatial pattern of the open water areas during the BCP events for 2009–2010, Hirano et al. (2016) considered the hybrid BCP area influenced by ocean heat flux as the region between Point Barrow and Wainwright. However, given the climatology of the spatial pattern of the SIP

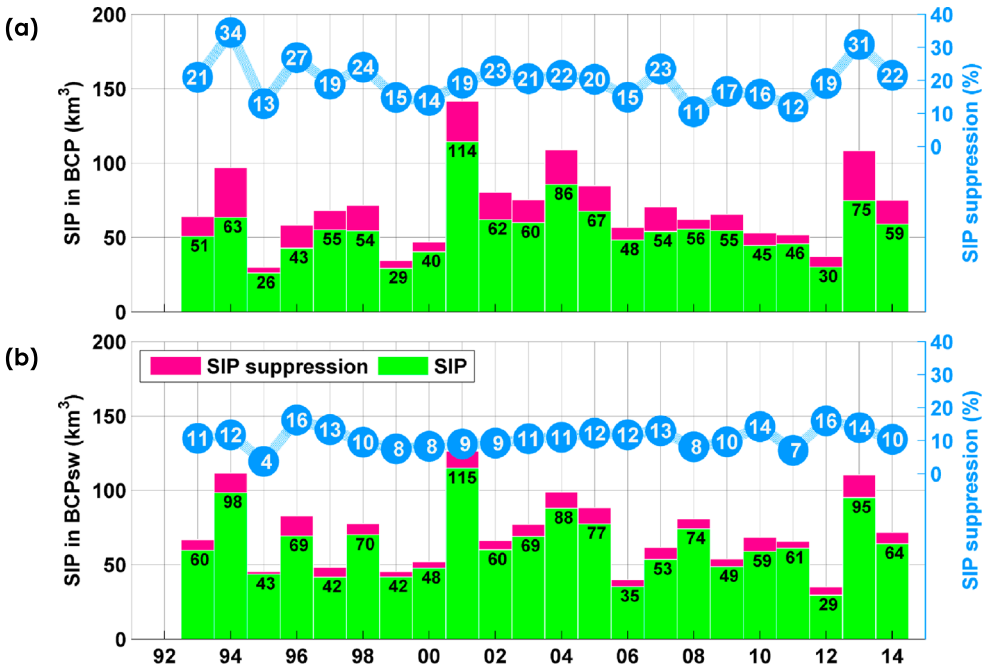

Figure 3. (a) Time series of cumulative SIP (green bars with numbers) and SIP suppression (pink bars) in the (a) BCP and (b) BCPsw from November to May for 1992–2014. Note that SIP suppression is stacked on SIP. The circles with numbers in both panels indicate fractions of SIP suppression. Areas of the BCP and BCPsw are shown in Figure 1b.

suppression (Figures 2c and 2d) and the observation that the upwelled AW reached at least to the region off Icy Cape (C1 in Figure 1b; Ladd et al., 2016), the hybrid BCP area identified in Hirano et al. (2016) underestimates the influence of higher ocean heat fluxes and SIP suppression through AW upwelling. Based on the climatological distributions of SIP and SIP suppressions (Figure 2), we define three separate coastal polynya areas along the Barrow Canyon pathway (shown by green boxes in Figure 2). The region between Cape Lisburne and Point Barrow, conventionally referred to as Chukchi polynya (e.g., Itoh et al., 2012; Winsor & Chapman, 2002), is divided into two coastal polynyas—one is the hybrid BCP influenced by the ocean heat flux from upwelled warm water through Barrow Canyon and the other one is BCPsw (southwest of BCP) polynya not much influenced by that ocean heat flux. In addition, the region between Bering Strait and Cape Lisburne is defined as BSne (northeast of Bering Strait) polynya, because the SIP in this polynya is also an important source of salt flux for the modification of Pacific-origin water.

3.3. Variability of SIP

Figure 3 shows time series of SIP and SIP suppression in the BCP and BCPsw in November–May for 1992–2014. Both SIP and SIP suppression occur in the BCP every year, demonstrating the consistent hybrid nature of BCP. The SIP and SIP suppression in the BCP and BCPsw show no statistically significant trends (based on the Mann-Kendall test even at 90% confidence level) or transitions (such as in the context of the record summer sea-ice extent minima beginning in 2007 and shorter ice seasons; e.g., Johnson & Eicken, 2016), but fluctuate from year to year. The highest and lowest SIP in the BCP since 1992 was found in 2000–2001 and 1994–1995, respectively. The fraction of SIP suppression ranges from 11 to 34% and exceeds 30% in 1993–1994 and 2012–2013. In the BCPsw, SIP is comparable to that in the BCP. Although the fraction of SIP suppression in the BCPsw is less than that in the BCP (Figures 2d and 3b), the BCPsw area is also sometimes influenced by the ocean heat flux from upwelled AW. This interpretation is supported by the observations of Ladd et al. (2016) and the distribution of Atlantic-water tracer (Figures 8e–8h) described in section 4.

3.4. Major Factors Controlling SIP Variability in the BCP

As noted in the previous section, SIP and SIP suppression in the hybrid BCP fluctuate from year to year, but there are no statistically significant trends (Figure 3a). Hirano et al. (2016) pointed out that the BCP events are triggered by northeasterly winds associated with variability in the strengths of Beaufort High (BH) and

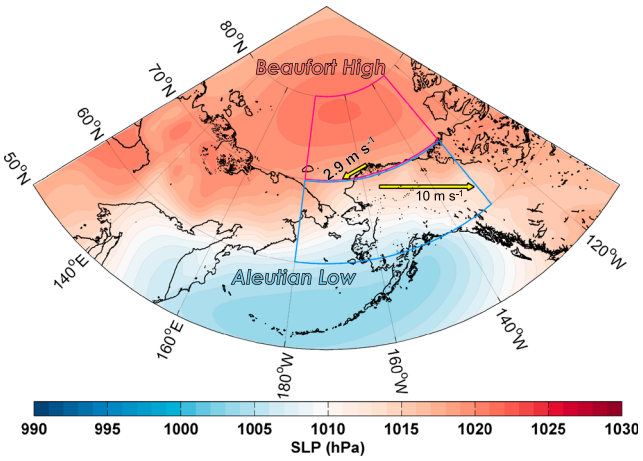

Figure 4. Mean sea level pressure (SLP, shade) and wind off Utqiaġvik (vector with its amplitude) from November to May for 1979–2014 in the Bering Sea and Pacific sector of the Arctic Ocean. The red and blue boxes represent BH (70–80°N, 180–230°E, altered Beaufort High Index by Hori et al., 2015) and AL (60–70°N, 180–230°E) regions, respectively.

Aleutian Low (AL) pressure systems. Here a major factor controlling the variability of SIP and SIP suppression in the BCP is analyzed using sea level pressure (SLP) and wind speed at 10 m height (U10 and V10) provided by the European Centre for Medium-Range Weather Forecasts (ECMWF) Interim Re-Analysis (ERA-Interim) for 1979–2014.

Figure 4 shows mean SLP in November–May for 1979–2014. The SLP pattern in November–May is climatologically characterized by distributions of AL over the Bering Sea and BH over the Canada Basin. In the same period, northeasterly wind off Utqiaġvik is associated with the SLP pattern (arrow in Figure 4). As with the SIP (Figure 3), the northeasterly wind off Utqiaġvik also fluctuates from year to year with no statistically significant trend (based on the Mann-Kendall test even at 90% confidence level). To examine atmospheric conditions with respect to their climatologies, area-averaged SLP in BH and AL regions (respectively defined in red and blue boxes in Figure 4), SLP difference between them and the northeasterly wind component off Utqiaġvik (hereafter along-BC wind) are standardized in November–May for 1979–2014 (see details in the caption of Figure 5). In November–May, along-BC winds and SLP differences are highly correlated (R^2 = 0.74). This indicates an association between along-BC wind and SLP difference, that is, north-south pressure gradient between BH and AL.

As examples for the lowest and highest SIP years (1994–1995 and 2000–2001, respectively), time series of the SLP difference, along-BC wind, SIP, and SIP suppression in the BCP are shown in Figure 5. In November–March, the negative along-BC wind for 2000–2001 (high SIP) is much stronger and more frequent compared to the climatology (Figure 5c). In contrast, the negative along-BC wind in 1994–1995 (low SIP) is far less frequent (Figure 5a). Daily SLP difference and along-BC wind are inversely correlated (Figures 5a and 5c). Further, variation of the along-BC wind is closely linked to the SIP and SIP suppression in the BCP (Figures 5b and 5d). The correlation coefficients between the strength of northeasterly winds and SIP (R_{SIP})/SIP suppression ($R_{SIPsupp}$) in the BCP are R_{SIP} = −0.43 and $R_{SIPsupp}$ = −0.29 for 1994–1995 and R_{SIP} = −0.76 and $R_{SIPsupp}$ = −0.49 for 2000–2001. Thus, the SIP and SIP suppression in the BCP are closely linked to frequency/strength of the northeasterly (negative along-BC) winds. A similar relationship between

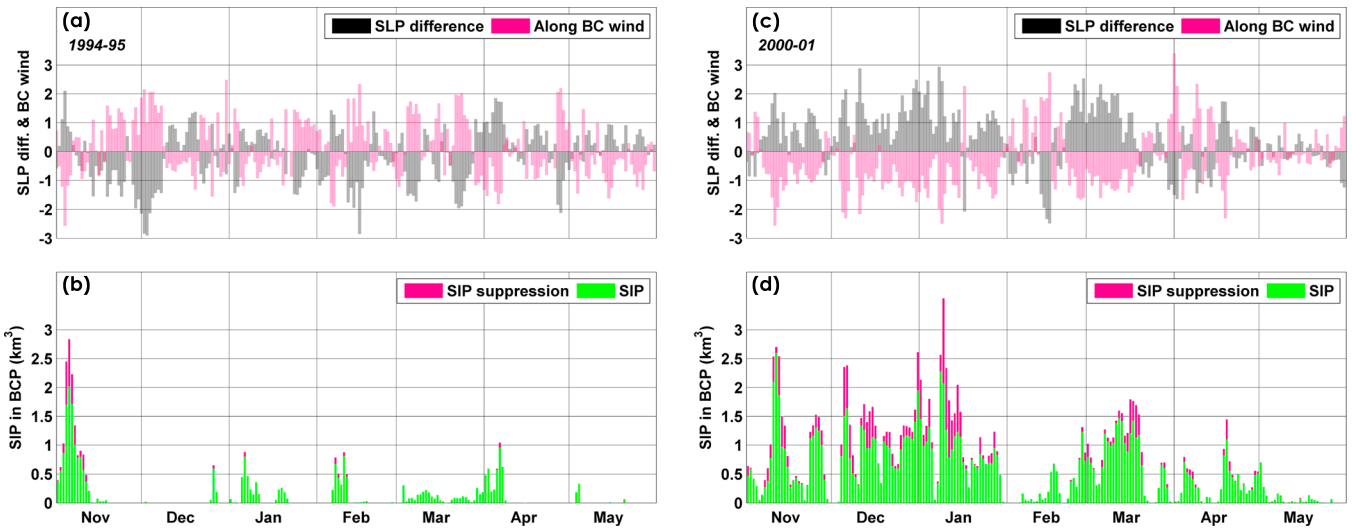

Figure 5. Time series of (a and c) standardized SLP difference between BH and AL (gray; BH minus AL; positive values represent the positive north-south pressure gradients) and along-BC wind (63°T: 0°T corresponds to the north; negative values represent the northeasterly winds) in the BCP (pink), and (b and d) SIP (green) and SIP suppression (pink) in the BCP from November to May for 1994–1995 and 2000–2001. The mean and standard deviation of the standardized parameters are 0 and 1, respectively. A value of 0 corresponds to climatology of each parameter for November–May (see section 3.4).

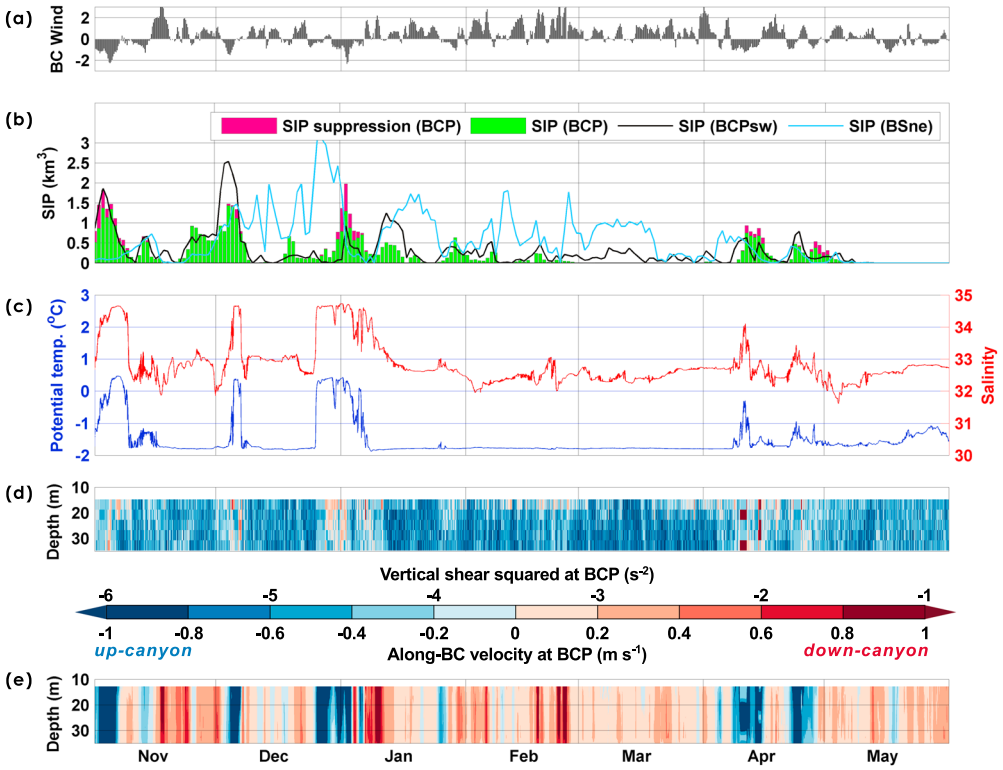

Figure 6. Time series of (a) standardized along-BC wind in the BCP, (b) SIP (green) and SIP suppression (pink) in the BCP, and SIP in the BCPsw (black) and BSne (light blue), (c) potential temperature (blue) and salinity (red) at 43 m, and vertical structures of (d) squared vertical shear and (e) along-BC velocity (63°T: 0°T corresponds to the north; positive values represent the down-canyon flows) from November to May for 2010–2011. Data shown in (c)–(e) are obtained at the BCP mooring.

the northeasterly winds over the Chukchi shelf and the pressure systems of BH and AL was discussed in Weingartner et al. (2017) stating abnormally large up-canyon transports in fall/winter are associated with strong AL and BH. They demonstrated that mean monthly up-canyon transport at the head of Barrow Canyon (BC2 in Figure 1b) was the maximum at ~0.7 Sv in January 2001. During the same period, the prevailing northeasterly wind resulted in high SIP and SIP suppression in the BCP (Figures 5c and 5d).

4. BCP Events for 2010–2011 and 2012–2013

Mooring observations in the BCP have been conducted without interruption since July 2009 and are ongoing (Figure 1b). Here we examine the characteristics of BCP events when the amounts of SIP and SIP suppression are relatively high in 2012–2013 (SIP: 75 km^3, SIP suppression: 33 km^3) and relatively low in 2010–2011 (SIP: 46 km^3, SIP suppression: 6 km^3; Figure 3a). We note that the year with the lowest SIP and SIP suppression was 2011–2012 after 2009 (Figure 3a), but unfortunately, the moored conductivity-temperature recorder failed for this period. Although the characteristics of individual BCP events in 2010–2011 and 2012–2013 are basically similar to those observed in 2009–2010 (Hirano et al., 2016), these two seasons exhibit distinct differences in frequency/strength of the negative along-BC wind, the cumulative amounts of SIP and SIP suppression, and ocean temperature, salinity, and currents (Figures 6 and 7). In 2010–2011, there were relatively few episodes of strongly negative along-BC winds and those that occurred lasted only for a few days (Figure 6a). By contrast, the along-BC wind in 2012–2013 was persistently and strongly negative from mid–December to mid–March (Figure 7a). As in 1994–1995 and 2000–2001 (Figure 5), daily SIP and SIP suppression are well correlated to variations of the northeasterly (negative along-BC) wind for both 2010–2011 ($R_{SIP} = -0.55$, $R_{SIPsupp} = -0.53$) and 2012–2013 ($R_{SIP} = -0.76$, $R_{SIPsupp} = -0.67$). However, SIP and SIP suppression occurred without northeasterly winds in November of 2012 (Figures 7a and 7b). During this period, the BCP region was not fully covered by sea ice (i.e., open water and/or thin ice region) and water temperature at subsurface

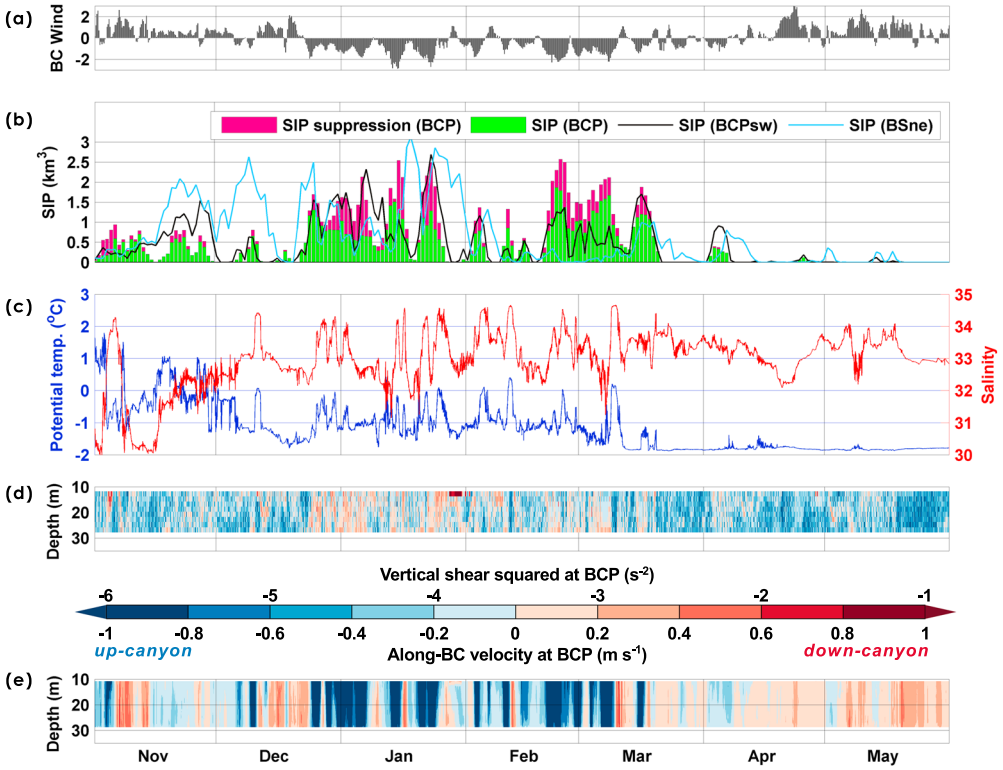

Figure 7. Similar to Figure 6 but for 2012–2013. (c) Potential temperature and salinity at 36 m.

never reached the freezing point (Figure 7c). As long as heat is lost from the ocean to the atmosphere, such sea-ice and ocean conditions result in SIP and SIP suppression without sea-ice divergence and upwelling of warm water caused by northeasterly winds. Note that such periods with SIP and/or SIP suppression without the northeasterly winds are not referred to as the BCP events. Once thicker ice covers the BCP region, SIP and SIP suppression are driven by northeasterly winds. This relationship is remarkable particularly between mid–December and mid–March in 2012–2013 (Figures 7a and 7b). It should be noted that it is difficult to evaluate a relative contribution to the hybrid BCP from the sea-ice divergence and upwelling, because it is not known exactly how ocean heat from the upwelled warm water spreads to contribute the SIP suppression using the BCP mooring data at a single point. When the along-BC wind was persistently negative, warm (>0 °C) and saline ($S > 34.0$) AW was upwelled (Figure 7c), strong up-canyon flow was established (Figure 7e), and the SIP was increasingly suppressed (Figure 7b). In this manner, the timing of warm water upwelling is consistent with that of the SIP suppression in the BCP. The moorings at the head of Barrow Canyon also observed the dominant up-canyon transport of 1 Sv in January and February 2013 under strong northeasterly winds over the northeastern Chukchi Sea (Weingartner et al., 2017). On the other hand, in 2010–2011, down-canyon flow was mostly dominant during November–May (Figure 6e), except for some periods with relatively strong northeasterly wind.

Figures 8a–8d show the spatial distributions of SIP and open water area in January–April of 2013. The model experiment demonstrates that the highest concentrations of the Atlantic-water tracer at the surface appear in the coastal region south and west of Point Barrow (Figures 8e–8g). The areas of high tracer concentration are highly consistent with the open water area identified by the open water mask (Figures 8a–8c and 8e–8g). This agreement indicates extensive SIP suppression caused by the upwelled AW in the BCP and the validity of the satellite-based open water mask applied to SSM/I-SSMIS data in the BCP. It is notable that on 15 April after weakening of northeasterly winds (Figure 7a), surface tracer concentrations were relatively high and confined mainly to the Alaska coastline (Figure 8h) despite the absence of detected open water (Figure 8d). This indicates the presence of shelf waters containing a large component of upwelled AW on the northeastern Chukchi shelf (see section 6).

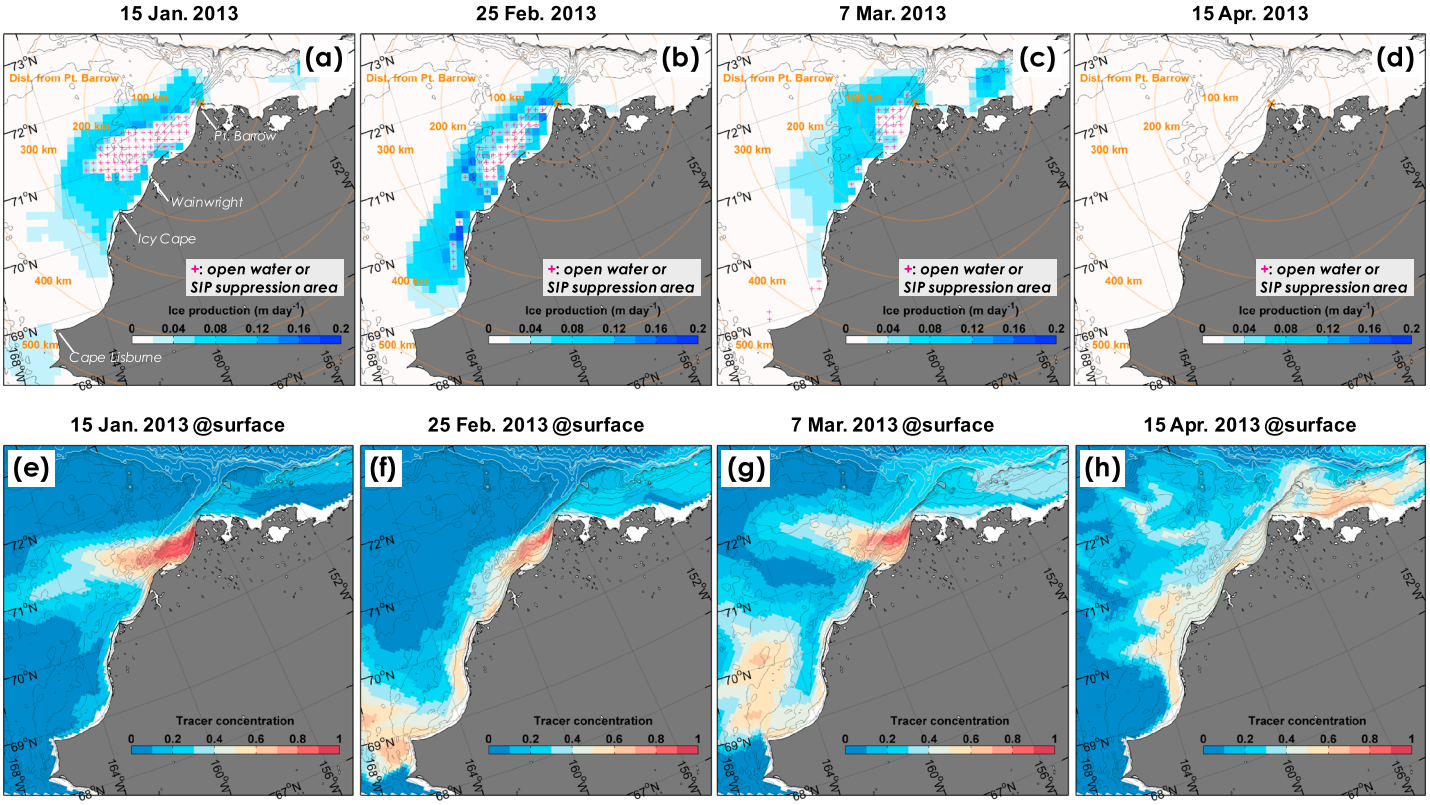

Figure 8. Spatial distributions of (a–d) SIP (shade) and open water or area of SIP suppression (hatched with plus sign) and (e–h) surface concentration of the Atlantic-water tracer (see the detailed release method in section 2.2). The daily fields on (a and e) 15 January, (b and f) 25 February, (c and g) 7 March, and (d and h) 15 April of 2013 are shown.

Although it is difficult to estimate the amount of sea-ice basal melt from satellite observations, it can be assumed that sea ice was melted by episodic temperature increases in the surface layer due to AW upwelling. Such a postulated relationship between the basal melt and upwelling of warm water would require verification by in situ observations using an ice mass balance buoy. Moreover, another important feature in the ocean during the BCP event is that vertical shear was enhanced compared with that in the other periods (Figures 6d and 7d). This indicates that vertical mixing was promoted by baroclinic current structure established after the upwelling (Hirano et al., 2016). The elevated vertical shear during the upwelling events was also observed off Icy Cape (Ladd et al., 2016; C1 in Figure 1b), suggesting the widespread vertical mixing on the shelf along the Alaska coast. The enhanced mixing on the shelf likely mixed the upwelled AW and shelf water masses, leading to ACWW formation (section 6).

The properties of ACWW passing through Barrow Canyon depend on the original salinity of PWW at the Bering Strait and the amount of additional salt input in the coastal polynyas along the pathway (Itoh et al., 2012; Winsor & Chapman, 2002). Therefore, variability of SIP in the BCPsw and BSne (Figure 1b) in addition to the BCP also has important effects on the PWW modifications. In both 2010–2011 and 2012–2013, SIP in the BCPsw and BSne was comparable to or higher than that in the BCP (Figures 3, 6b, and 7b). Variability of SIP in the BCPsw approximately coincided with that of the BCP. Possibly, this is a result of sea-ice divergence in the BCP and BCPsw being induced by the same northeasterly winds, given the similar coastline orientations. In contrast, SIP in the BSne did not necessarily match that of the other two regions likely due to the different coastline orientation (Figures 6b and 7b).

After entering the Chukchi shelf, PWW likely experienced a variety of modification processes along the Barrow Canyon pathway such as additional salt input (due to brine rejection) accompanied by SIP in the coastal polynyas and ocean heat flux from the upwelled AW in the BCP, and the significantly modified form of PWW eventually passed through Barrow Canyon. In terms of the additional salt input, BCPsw and BSne

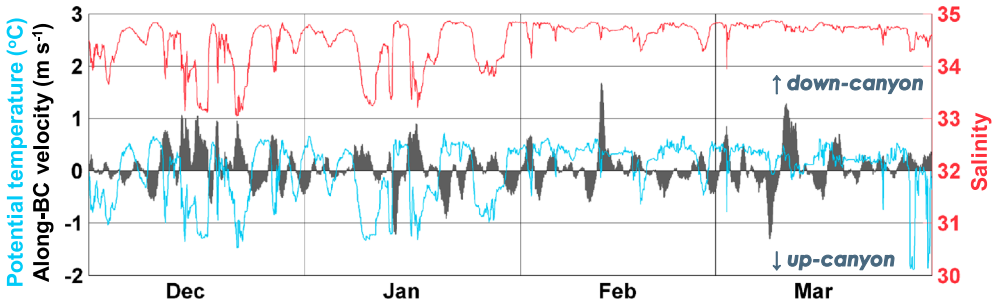

Figure 9. Time series of potential temperature (light blue), salinity (red), and along-BC velocity (black bar, 63°T: 0°T corresponds to the north; positive values represent the down-canyon flows) at 182 m of BCC mooring in Barrow Canyon from December 2012 to March 2013.

polynya activities should remotely influence ACWW formation (in particular, polynya water production) because SIP in these coastal polynyas is comparable to or higher than in the BCP (Figures 2, 3, 6, and 7). The following section describes water properties of ACWW observed in Barrow Canyon.

5. ACWW Properties Observed in Barrow Canyon

As mentioned above, the possible PWW modifications along the Barrow Canyon pathway may originate not only from the BCP but also from the upstream coastal polynyas (BCPsw and BSne). In addition, the BCP mooring is located northeast (downstream) of the head of Barrow Canyon on the shallower shelf beside the Barrow Canyon, suggesting that winter waters densified in the coastal polynyas flow directly into Barrow Canyon without going through the BCP mooring site. Therefore, the data obtained at BCC (Figure 1b and Table 2) are also used to examine the properties of ACWW passing through Barrow Canyon.

Figure 9 shows time series of potential temperature and salinity along with along-BC velocity at 182 m depth of BCC from December 2012 to March 2013 when AW was frequently upwelled onto the shelf over the BCP (Figure 7). During this period, magnitudes of down- and up-canyon flows at BCC reached >1 m/s. At this depth, temperature and salinity (hence density) increased during up-canyon flows, related to the AW inflow from the Canada Basin onto the shelf. When the currents shifted to the down-canyon flows, on the other hand, temperature and salinity became lower than those during up-canyon flows. The variation ranges of the properties between down- and up-canyon flows were relatively large until February, and then they subsequently became smaller. This is considered to reflect a history of modification processes that the upwelled AW has experienced over the shelf. The large range of variation suggests ongoing mixing of the upwelled AW with cold, fresh (less dense) water on the shelf, while the smaller range suggests mixing of the upwelled AW with shelf waters consisting of a large amount of AW previously transported onto the shelf.

At shallower BCC depths (44, 83, and 121 m), distinct changes in water properties between up- and down-canyon flows are also evident (Figures 10a–10f). After mid-March when up-canyon flows in the BCP (Figure 7) and BCC (Figure 9) decline, near-freezing temperature water with a range of salinities occurred at BCC (Figures 10a, 10c, 10e, and 10g). Especially below 120 m depth at BCC, hypersaline polynya water ($T \sim T_f$, $S > 34.0$) dense enough to sink to or below lower halocline level in the Arctic basin was observed during down-canyon flows after April (Figures 10e and 10g). Such hypersaline polynya water may form through additional salt input from brine rejection accompanying SIP along the Alaska coast. In addition, Mirai2013 hydrographic data (black crosses in Figure 10) indicate that water properties of the lower halocline layer (transition layer from θ_{min} to θ_{max}) in the southern Canada Basin and CBL regions are similar to those observed during the down-canyon flows at BCC in January–February (Figures 10c, 10e, and 10g; see section 7.1).

6. ACWW Formation Processes

Here the formation of different types of ACWW is examined from the perspective of water modification processes. Figure 11 shows potential temperature-salinity relationships in Bering Strait (A4W), BCP, and Barrow Canyon (BCC) for 2010–2011 and 2012–2013. In Bering Strait, water properties for these two years are nearly the same, with salinities up to ~33.0 and temperatures near the freezing point. In the BCP and BCC downstream, however, water properties observed in the two years are distinctly different. In 2010–2011,

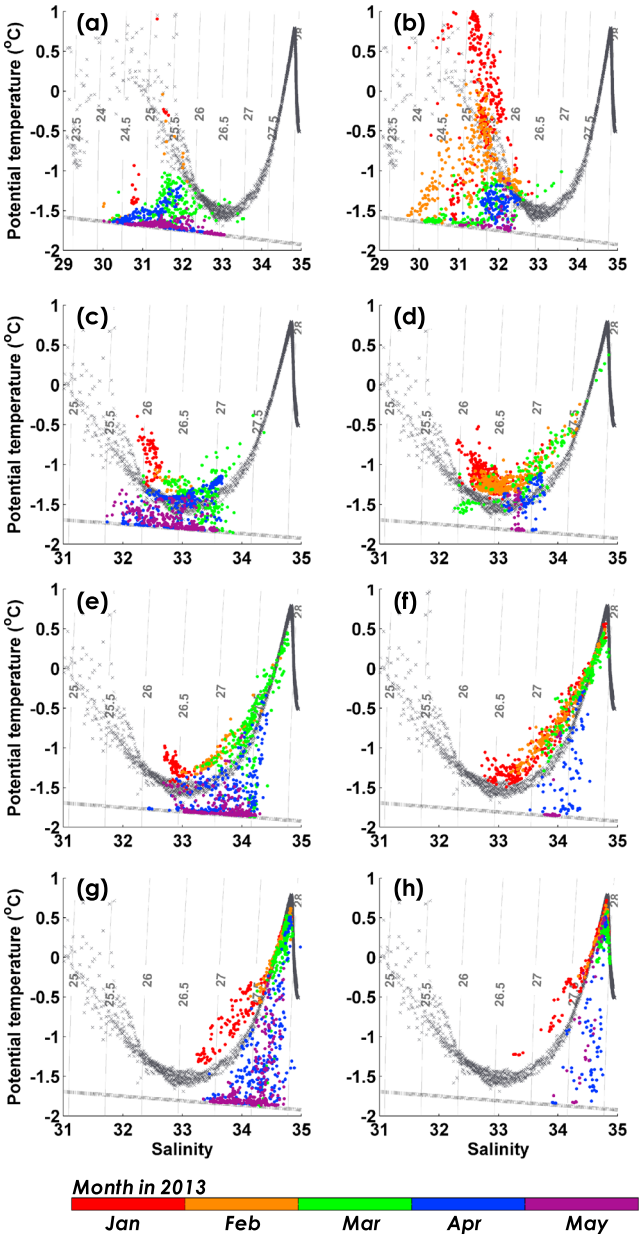

Figure 10. Relationship between potential temperature and salinity during down- and up-canyon flows from January to May 2013 at (a and b) 44 m, (c and d) 83 m, (e and f) 121 m, and (g and h) 182 m of BCC mooring in Barrow Canyon. The black crosses represent the data from Mirai2013 hydrographic data (locations are shown by purple squares in Figure 1a). Note that the left (right) panels show data during down- (up-) canyon flow. The gray contours denote potential density surfaces, and nearly horizontal gray lines are the freezing point of seawater at atmospheric pressure. Data are plotted with different colors depending on months of observation shown in the color bar.

salinities in the BCP and BCC were higher than those in Bering Strait but they increased to ~34.0 at most and their occurrence was rare (Figure 11a), indicating the low contribution of brine rejection to the production of hypersaline polynya water. In 2012–2013, by contrast, salinities in the BCP and BCC were significantly higher than those in Bering Strait (Figure 11b), indicating the high contribution of brine rejection to the production of hypersaline polynya water. The differences in salinity increases for these two years are attributed to the differences in the amounts of SIP in the coastal polynyas along the Barrow Canyon pathway (Figures 3, 6b, and 7b). Another difference is the presence of two mixing lines extending from AW, between AW and PWW and between AW and polynya water (Figure 11c). In 2010–2011, only a mixing process along the AW-PWW mixing line was prominent (Figure 11a). In 2012–2013, mixing processes along mixing lines of AW-PWW and AW-polynya water were both prominent (Figure 11b), but both mixing processes did not dominate simultaneously as described below.

The AW-PWW mixing line in 2012–2013 was prominent in January–February (red and orange dots in Figures 10e and 10g). After the northeasterly winds weakened in mid–March, the AW-Polynya water mixing line subsequently became prominent, then export of polynya water or water along the AW-Polynya water mixing line to the basin dominated after April (blue and purple dots in Figures 10e and 10g). The mooring-based data and model-simulated results can explain the transition of the two mixing processes along these two mixing lines extending from AW. From late December 2012 to mid–March 2013 when AW upwelling frequently occurred (Figure 7c), the simulated tracer distribution suggests that the upwelled AW was transported over a wide area of the northeastern Chukchi shelf along the Alaska coast (Figures 8e–8g). The amount of oceanic heat from the upwelled warm water onto the eastern Chukchi shelf is likely associated with the total duration of the BCP events, influencing on the ACWW formation. During this period, the upwelled AW mixed with PWW (i.e., following the AW-PWW mixing line) on the shelf, where the vertical (diapycnal) mixing was enhanced (Figure 7d). In mid-March, down-canyon flows became dominant on the shelf (Figure 7e) due to weakening of the northeasterly winds (Figure 7a). After mid-March, a large amount of upwelled AW that had transported onto the shelf also mixed diapycnally and/or isopycnally with hypersaline polynya water formed over the coastal polynyas (i.e., following the AW-Polynya water mixing line) because their densities are close to each other (Figure 11c). Then, the mixture was transported toward Barrow Canyon. The distribution of elevated concentrations of the Atlantic-water tracer along the Alaska coast (Figure 8h) suggests the presence of the mixture of AW and polynya water and its transport toward the northeast.

The BCP mooring did not observe the water along the AW-Polynya water mixing line and the most saline polynya water (Figure 11b). From March to May 2013, polynya waters showed salinities $S > 35.0$ at BC2 in the upstream region of the head of Barrow Canyon (Weingartner et al., 2017, in their Figure 13) and $S \sim 34.5$ at BCC at the mouth of Barrow Canyon (Figure 10g). In contrast, the salinity of polynya water at BCP did not exceed 34.0 (Figure 7c). Therefore, it is highly likely that the saline (dense) waters produced over the BSne and BCPsw in the upstream region of the head of Barrow Canyon directly flowed into Barrow Canyon without passing through the BCP mooring site on the shallower shelf beside the Barrow Canyon.

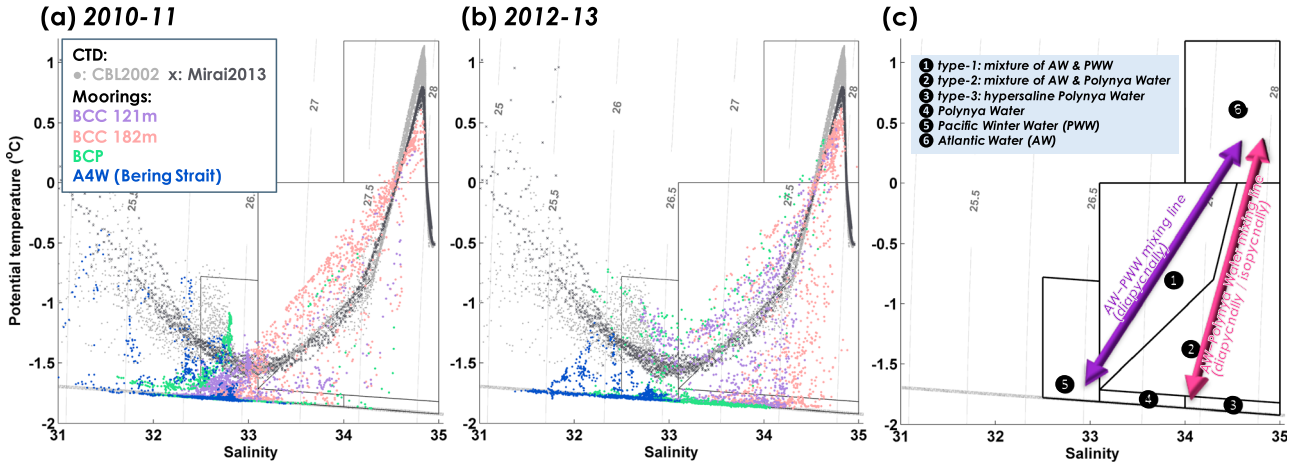

Figure 11. Relationship between potential temperature and salinity for (a) 2010–2011 and (b) 2012–2013 at 121 m of BCC (purple), 182 m of BCC (pink), 43 m for 2010–2011 (36 m for 2012–2013) of BCP (green), and 45 m of A4W (blue). Data at the A4W are shown for the period from December to May. Data at the BCP and BCC are shown only during down-canyon flows in January to May. The gray dots and black crosses represent the data from CBL2002 (magenta circles in Figure 1a) and Mirai2013 (purple squares in Figure 1a), respectively. (c) Water boundaries (Table 1) and mixing lines associated with ACWW formation. Enclosed area by thick black lines indicates the boundaries: type-1 ACWW (mixture of AW and PWW, labeled "1"), type-2 ACWW (mixture of AW and polynya water, labeled "2"), type-3 ACWW (hypersaline polynya water, labeled "3"), polynya water (labeled "4"), Pacific Winter Water (PWW, labeled "5"), and Atlantic Water (AW, labeled "6"). The purple and pink arrows represent AW-PWW and AW-polynya water mixing lines, respectively.

Three types of ACWW are formed along the Barrow Canyon pathway; type-1: a mixture of AW and PWW, type-2: a mixture of AW and polynya water, and type-3: hypersaline polynya water. Considering the water properties and mixing lines associated with the ACWW formation, we define each of the three ACWW types with a reference to the water properties of a lower halocline layer in the basin (Table 1 and Figure 11c) as follows; type-1 ($S > 33.1$ and lower halocline temperature $< T < 0.0$), type-2 ($S > 33.1$–34.5 and $T_f + 0.1 < T <$ lower halocline temperature), and type-3 ($S > 34.0$ and $T < T_f + 0.1$). The definitions for type-1 and type-2 ACWWs are not strictly mutually exclusive in terms of their temperatures due to their complex characteristics. In the definitions, the "lower halocline temperature" serves as a measure rather than a unique temperature value; temperature warmer (colder) than the lower halocline temperature is presumably caused by more influence of warm AW (cold polynya water) on their formation on the shelf. In addition, type-1 and type-2 ACWWs overlap on the temperature-salinity space (Figure 11). However, these ACWW varieties are intrinsically different because they formed through different mixing processes (type-1: diapycnal mixing; type-2: diapycnal and/or isopycnal mixing) during different periods (Figures 10e and 10g).

Although ventilation for water with $S > 33.1$ had been previously attributed to hypersaline polynya waters (Shimada et al., 2005; Weingartner et al., 1998), Woodgate, Aagaard, Swift, et al. (2005) suggested that much of the western Arctic's lower halocline is influenced by diapycnal mixing of PWW ($S \sim 33.1$) and denser AWs, with such mixing taking place possibly over the northern Chukchi shelf/slope. During a prolonged up-canyon transport event from December 2012 to February 2013, only colder (< -1 °C) and fresher (<33.1) waters were observed at the head of Barrow Canyon (BC2 in Figure 1b; Weingartner et al., 2017). However, the lower halocline water and/or AW found at a deeper layer are thought to be upwelled onto the shelf at the BCP (Figure 7c), since the properties of observed upwelled waters were often $T > 0$ °C and $S > 34.0$. Differences in water properties observed at the BCP and at the head of the canyon (BC2; Weingartner et al., 2017) might be explained by the fact that the upwelled water was confined along the coast and/or that the upwelled water was modified before reaching the head of the canyon.

7. Discussion

7.1. Possible ACWW Spreading Paths Into Interior Arctic

As mentioned in section 5, water properties of the lower halocline layer in the southern Canada Basin and CBL regions are similar to those of type-1 observed during the down-canyon flows at BCC (Figures 10c, 10e, and 10g). Although observation years are different, Figure 11b also shows that water properties of the lower halocline water (gray dots) in the diapycnally ventilated region in the CBL (magenta dots in Figure 1a) are similar

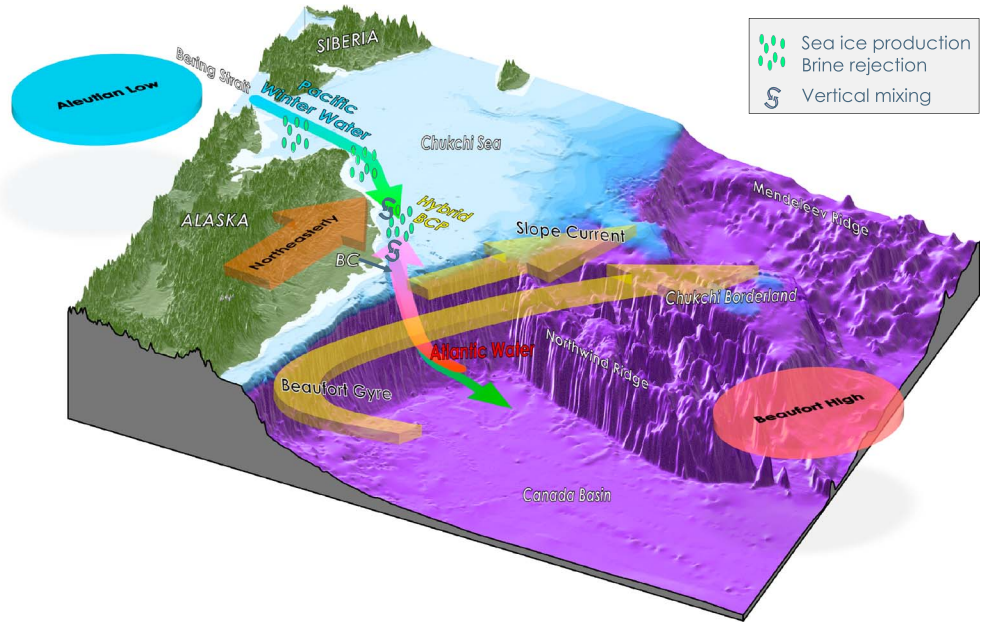

Figure 12. A schematic showing the formation processes of Alaskan Coastal Winter Water (ACWW) over the eastern Chukchi shelf (along the Barrow Canyon pathway) and its spreading paths into the interior Arctic. Much of ACWWs are more likely to spread into the regions especially over the Chukchi Borderland, the Northwind Ridge, and the southern Canada Basin with the Slope Current and/or Beaufort Gyre represented by broad yellow arrows. As for denser type-2 and type-3 waters among ACWWs, part of them potentially intrudes at depths comparable to or deeper than the AW layer in the Canada Basin represented by green arrow.

to those of type-1 ACWW formed by the mixing of AW with PWW (as observed in January 2013; Figures 10e and 10g). In addition, corresponding lower halocline waters along the AW-PWW mixing line was found over the CBL, Northwind Ridge, and southern Canada Basin (McLaughlin et al., 2004). A particle tracing calculation with satellite-based geostrophic velocity conducted by Mizobata et al. (2016) showed that the Pacific-origin water exported north of Barrow Canyon is usually transported to the CBL via the Beaufort Gyre (BG). They also indicated that the pathway of the passive tracer in the winter of 2012–2013 was different from that in the other winters, where the tracer was transported to the western side of Barrow Canyon (shelf break) or the northern shelf of the Chukchi Sea because of the expansion and intensification of the BG in conjunction with the prevailing northeasterly wind over the Chukchi Sea shelf (see their Figure 12). An important point here is that the BG during winter is highly variable in its strength and circulation pattern in response to wind strength and pattern (Mizobata et al., 2016). In addition, Corlett and Pickart (2017) recently showed that a substantial part of Pacific-origin water exported from Barrow Canyon is transported westward over the upper continental slope via the Chukchi slope current emanating from the canyon. It should be noted that the Chukchi slope current is quantified based on historical hydrographic and velocity sections occupied in warm seasons (May–October; Corlett & Pickart, 2017).

Considering all the results from the previous and current studies, we propose ACWW formation processes along the eastern Chukchi shelf and subsequent spreading paths into the basin (Figure 12). Three types of ACWW are formed through different modification processes that PWW has experienced over the shelf along the Barrow Canyon pathway, such as SIP, upwelling of AW, and mixing processes. It is worthwhile to mention that the formation and properties of each ACWW are involved with various spatial and temporal evolutions. For type-1 (mixture of AW and PWW) and type-2 (mixture of AW and polynya water) waters, they are formed through a local contribution from warm AW upwelling mainly onto the BCP (i.e., spatial evolution). Water property of type-2 is additionally influenced by a remote contribution from a salt input through SIP in the upstream BCPsw and BSne polynyas, because the type-2 property is dependent on that of polynya water mixed with upwelled AW (i.e., spatial and temporal evolutions). Type-3 of hypersaline polynya waters is mainly formed through local and remote contributions from a salt input through SIP in the coastal polynyas all the way along the Barrow Canyon pathway (i.e., temporal evolution). After passing through Barrow

Canyon, it is suggested that much of ACWWs are more likely to flow westward (along the shelf break/slope of the Chukchi Sea) or northwestward (toward the Northwind Ridge and CBL regions via the southern Canada Basin) with the slope current and/or BG. Therefore, much of ACWW is a potential source water for the formation and maintenance of the lower halocline layer especially over the CBL, Northwind Ridge, and southern Canada Basin (Figure 12). Further, it remains possible that denser type-2 and type-3 waters among ACWWs directly intrude at depths comparable to or deeper than the AW layer in the basin because its density is close to AW in the basin (Figure 11c). The transports associated with these three ACWW types could be quantified using the model outputs. However, the simulated transports contain significant biases partly because our model underestimated the AW temperature (Watanabe et al., 2017). However, impacts of the cold bias of AW on our conclusion about the AW-influence on the ACWW formation are minor.

7.2. Atlantic Influence on the Eastern Chukchi Shelf in Winter

Even in the Pacific sector of the Arctic Ocean, as Woodgate, Aagaard, Swift, et al. (2005) also suggested, the properties of ACWW that eventually enters the Arctic basin are strongly affected by the Atlantic-origin waters. The region influenced by the upwelled AW covers an area extending more than 200 km southwestward from Point Barrow along the eastern Chukchi shelf to Icy Cape (Figure 8). Although Weingartner et al. (2017) showed that only about one third of the up-canyon events transported the warm upwelled water observed by their EBC mooring near Utqiaġvik (~110 km northeast of BC2; see their Figure 14) to the head of Barrow Canyon, this is likely because their conclusions were based on the mooring data obtained in 2010–2011 and 2011–2012 when there were few episodes of strong northeasterly winds as indicated by low SIP and SIP suppression shown in Figure 3. Except for the hypersaline polynya water (type–3), the ACWW formation process can be considered as a modification process of upwelled AW onto the shelf. The upwelled AW is modified by mixing processes on the shelf and returns to the basin to ventilate there (Figures 10 and 11). Jackson et al. (2015) examined the formation process of Beaufort Shelf Winter Water (BSWW) on the Canadian Beaufort shelf, occupied by low salinity shelf water (S ~ 20–25) in summer. They found that the upwelled saline, Atlantic-origin water plays an important role in BSWW formation in upwelling-favorable years, preconditioning the shelf region for saltier BSWW formation. Enhancing our understanding of the formation and maintenance of a cold halocline layer in the Pacific sector of the Arctic basin requires future work that considers both Pacific and Atlantic influences on winter water formation across the entire region from the Canadian Beaufort shelf to Chukchi shelf.

Even without oceanographic observations, the ACWW formation processes proposed by the present study qualitatively allow us to infer the ACWW properties entering the interior Arctic every year, based on variabilities of SIP and SIP suppression (indicative of the thermodynamic influence of AW upwelling; Figure 3). For example in 1993–1994, 2000–2001, and 2003–2004, high SIP and active upwelling might be potential factors to form large amounts of all types of ACWW widely contributing to basin ventilation at various depths. On the other hand, in 1994–1995, 1998–1999, and 2011–2012, PWW might have flowed into the basin without much modification along the Barrow Canyon pathway because of low SIP and inactive upwelling.

We have demonstrated that upwelled AW suppresses SIP in the BCP and alters the ACWW formation process. However, the upwelled AW undoubtedly exerts influence on basal melt and/or inhibition of ice growth in the ice-covered area, because the upwelled AW spreads over a wide area on the eastern Chukchi shelf centered along the northern Alaska coast (Figure 8). Thus, this study may offer further insights into variability of sea-ice volume (in other words, a product of area and thickness of sea ice) and associated freshwater budget over the eastern Chukchi shelf. At this point, although it is difficult to estimate the amount of sea-ice basal melt by satellite observations, model results not shown in this paper suggest that upwelled AW can lead to basal melt of sea ice. Further verification of links between AW upwelling and bottom ice melt is needed.

A key finding is the absence of any significant trend or transition in the magnitude of either SIP or SIP suppression between 1992 and 2014. With delays in fall freezeup and earlier onset of break-up, Johnson and Eicken (2016) found significant reductions in the length of the ice season in the eastern Chukchi and western Beaufort Seas. Based on their findings, we expect a reduction in the ice season length by a month or more over the time period of this study. The magnitude of SIP is instead related to the year-to-year fluctuation of winter northeasterly wind stress off Utqiaġvik without any long-term trends. Another potential factor includes a more mobile sea-ice cover (Hutchings & Rigor, 2012) that supports dynamic ice production in polynyas, helping offset overall reductions in ice season length and potential for heat loss over open water and

thin ice. Once the BCP region is fully covered with sea ice, ice divergence is still driven by northeasterly winds, but may increase in magnitude due to increased ice mobility. As a result, surface offshore Ekman transport followed by the upwelling of warm water would also be enhanced since wind stress on the ocean surface will likely increase over more widespread areas of open water and thin ice, relative to areas of thicker pack ice. Thus, it is presumed that warm water upwelling would exert a more significant impact on the ACWW formation if offshore sea ice becomes more mobile in a changing climate.

8. Summary

This study examined the water properties and formation processes of ACWW through the different modification processes that PWW experiences along the Barrow Canyon pathway, by using mooring data (in Bering Strait, BCP, and Barrow Canyon), estimates of SIP derived from SSM/I-SSMIS data, a model result, and hydrographic data obtained in the southern Canada Basin and CBL regions. The SIP along the Alaska coast shows no statistically significant trends (Figure 3). Instead, it is found that the SIP and SIP suppression fluctuate from year to year. PWW can be modified along the Barrow Canyon pathway by one or more of the following processes: SIP in the coastal polynyas, upwelling of AW centered in the BCP, and mixing processes on the shelf. Three different types of ACWW are formed along the Barrow Canyon pathway, and they intrude at the intermediate and deep layers of the Arctic basin: (i) a mixture of AW and PWW, (ii) a mixture of AW and polynya water, and (iii) hypersaline polynya water. Differences in water properties among ACWW varieties are attributed to differences in the modification processes that PWW has experienced on the eastern Chukchi shelf. The northeasterly winds over the BCP area, correlated with the north-south pressure gradient between BH and AL, are a common trigger of SIP and upwelling of AW (especially in the BCP) influencing ACWW properties. PWW modification processes around Barrow Canyon are more complicated than what occurs elsewhere in the Chukchi Polynya, because the northeasterly winds both promote and suppress SIP in the BCP. The impact of AW upwelling on the ACWW formation is most prominent in the BCP, usually confined along the coast. The PWW modifications in the eastern Chukchi shelf result in ACWW formation that eventually contributes to ventilation of intermediate and deeper layers in the Arctic basin. Even in the Pacific sector of the Arctic Ocean, the ACWW properties are strongly influenced by both Atlantic-origin and Pacific-origin waters. Further understanding of both Pacific and Atlantic influences on the winter water formation across the entire region from the Canadian Beaufort shelf to Chukchi shelf is crucial to elucidate variabilities of heat and freshwater budgets as well as an amount of sea ice in the Pacific sector of the Arctic Ocean.

Acknowledgments
We thank UIC Science and CH2MHill Polar Services for planning and field support in mooring operations off Utqiaġvik and the North Slope Borough Department of Wildlife Management for use of their boat and assistance from J. Craig George. We also thank Chris Petrich and Haruhiko Kashiwase for field assistance. The SSM/I-SSMIS data were provided by the National Snow and Ice Data Center (NSIDC), University of Colorado. The ERA-Interim data were obtained from the ECMWF Research Data Server (http://data.ecmwf.int/data/). The temperature-conductivity and temperature-pressure data and Acoustic Doppler Current Profiler (ADCP) data at the BCP mooring off Barrow are available at https://arcticdata.io/catalog/#view/doi:10.18739/A2PQ0M and https://arcticdata.io/catalog/#view/doi:10.18739/A2MT1D, respectively. The BCC mooring data in Barrow Canyon are available at http://www.jamstec.go.jp/arctic/data_archive_work/mooring/mooring_dataregist.html. The A4W mooring data in Bering Strait are available at https://data.nodc.noaa.gov/cgi-bin/iso?id=gov.noaa.nodc:0138583 for 2010-2011 and https://data.nodc.noaa.gov/cgi-bin/iso?id=gov.noaa.nodc:0138173 for 2012-2013. The CBL 2002 and Mirai2013 hydrographic (CTD) data are available at https://data.nodc.noaa.gov/cgi-bin/iso?id=gov.noaa.nodc:0138173 and http://www.godac.jamstec.go.jp/darwin/e, respectively. The model experiment was carried out using the Earth Simulator of Japan Agency for Marine-Earth Science and Technology (JAMSTEC). We are also grateful to Yasutaka Yamauchi for his processing of the ADCP data from the BCP moorings and Kohei Mizobata for his useful comments. In Japan, support was provided by Grants-in-Aids for Scientific Research (20221001, 23654163, 26800248, and 15H03721), the Green Network of Excellence (GRENE) Arctic Climate Change Research Project, and Arctic Challenge for Sustainability (ArCS) project of the Ministry of Education, Culture, Sports, Science and Technology, a research fund for Global Change Observation Mission 1st-Water of the Japan Aerospace Exploration Agency (JAXA), the Joint Research Program of the Institute of Low Temperature Science, Hokkaido University, Global Station for Arctic Research, a project of Global Institution for Collaborative Research and Education at Hokkaido University, and the Joint Research Program of the Japan Arctic Research Network Center. In the United States, support was provided by the National Science Foundation Seasonal Ice Zone

References

Aagaard, K., Coachman, L. K., & Carmack, E. (1981). On the halocline of the Arctic Ocean. *Deep-Sea Resesrch, Part A*, *28*(6), 529–545. https://doi.org/10.1016/0198-0149(81)90115-1

Aagaard, K., & Roach, A. T. (1990). Arctic ocean-shelf exchange: Measurements in Barrow Canyon. *Journal of Geophysical Research*, *95*(C10), 18,163–18,175. https://doi.org/10.1029/JC095iC10p18163

Bitz, C. M., & Lipscomb, W. H. (1999). An energy-conserving thermodynamic model of sea ice. *Journal of Geophysical Research*, *104*(C7), 15,669–15,677. https://doi.org/10.1029/1999JC900100

Cavalieri, D. J., & Martin, S. (1994). The contribution of Alaskan, Siberian, and Canadian coastal polynyas to the cold halocline layer of the Arctic-Ocean. *Journal of Geophysical Research*, *99*(C9), 18,343–18,362. https://doi.org/10.1029/94JC01169

Corlett, W. B., & Pickart, R. S. (2017). The Chukchi slope current. *Progress in Oceanography*, *153*, 50–56. https://doi.org/10.1016/j.pocean.2017.04.005

Eicken, H., Gradinger, R., Heinrichs, T., Johnson, M., Lovecraft, A., Fukamachi, Y., et al. (2011, Updated 2014). Mooring Temperature/Conductivity & Temperature/Pressure data (SIZONET). UCAR/NCAR–CISL–ACADIS. https://doi.org/10.5065/D6BG2KW9

Fukamachi, Y., Ohshima, K. I., Simizu D., Takatsuka, T., Iwamoto, K., Mahoney, A., et al. (2011, Updated 2014). Mooring ADCP data (SIZONET). UCAR/NCAR–CISL–ACADIS. https://doi.org/10.5065/D6G44N6Q

Godin, G. (1972). *The analysis of tides* (p. 264). Liverpool: Liverpool University Press.

Hasumi, H. (2006). CCSR Ocean Component Model (COCO) version 4.0. In *Center for Climate System Research Report* (Vol. 25, 103 pp.). Tokyo, Japan: University of Tokyo.

Hirano, D., Fukamachi, Y., Watanabe, E., Ohshima, K. I., Iwamoto, K., Mahoney, A. R., et al. (2016). A wind-driven, hybrid latent and sensible heat coastal polynya off Barrow, Alaska. *Journal of Geophysical Research: Oceans*, *121*, 980–997. https://doi.org/10.1002/2015JC011318

Hori, M. E., Inoue, J., & Kikuchi, T. (2015). The role of cyclone activity in the interannual variability of the summer time Beaufort High. *SOLA*, *11*(0), 104–107. https://doi.org/10.2151/sola.2015-025

Hunke, E., & Dukowicz, J. K. (1997). An elastic-viscous-plastic model for sea ice dynamics. *Journal of Physical Oceanography*, *27*(9), 1849–1867. https://doi.org/10.1175/1520-0485(1997)027<1849:AEVPMF>2.0.CO;2

Hutchings, J. K., & Rigor, I. G. (2012). Role of ice dynamics in anomalous ice conditions in the Beaufort Sea during 2006 and 2007. *Journal of Geophysical Research*, *117*, C00E04. https://doi.org/10.1029/2011JC007182

Itoh, M., Nishino, S., Kawaguchi, Y., & Kikuchi, T. (2013). Barrow Canyon volume, heat, and freshwater fluxes revealed by long-term mooring observations between 2000 and 2008. *Journal of Geophysical Research: Oceans*, *118*, 4363–4379. https://doi.org/10.1002/jgrc.20290

Observing Network award OPP-0856867 and the U.S. Department of Homeland Security Center for Island, Maritime and Extreme Environment Security (CIMES). Valuable comments and suggestions from two anonymous reviewers are greatly appreciated.

Itoh, M., Shimada, K., Kamoshida, T., McLaughlin, F., Carmack, E., & Nishino, S. (2012). Interannual variability of Pacific Winter Water inflow through Barrow Canyon from 2000 to 2006. *Journal of Oceanography*, *68*(4), 575–592. https://doi.org/10.1007/s10872-012-0120-1

Iwamoto, K., Ohshima, K. I., & Tamura, T. (2014). Improved mapping of sea ice production in the Arctic Ocean using AMSR-E thin ice thickness algorithm. *Journal of Geophysical Research: Oceans*, *119*, 3574–3594. https://doi.org/10.1002/2013JC009749

Iwamoto, K., Ohshima, K. I., Tamura, T., & Nihashi, S. (2013). Estimation of thin ice thickness from AMSR-E data in the Chukchi Sea. *International Journal of Remote Sensing*, *34*(2), 468–489. https://doi.org/10.1080/01431161.2012.712229

Jackson, J. M., Carmack, E. C., McLaughlin, F. A., Allen, S. E., & Ingram, R. G. (2010). Identification, characterization, and change of the near-surface temperature maximum in the Canada Basin, 1993-2008. *Journal of Geophysical Research*, *115*, C05021. https://doi.org/10.1029/2009JC005265

Jackson, J. M., Melling, H., Lukovich, J. V., Fissel, D., & Barber, D. G. (2015). Formation of winter water on the Canadian Beaufort shelf: New insight from observations during 2009–2011. *Journal of Geophysical Research: Oceans*, *120*, 4090–4107. https://doi.org/10.1002/2015JC010812

Johnson, M., & Eicken, H. (2016). Estimating Arctic sea-ice freeze-up and break-up from the satellite record: A comparison of different approaches in the Chukchi and Beaufort Seas. *Elementa Science Anthropocene*, *4*, 124. https://doi.org/10.12952/journal.elementa.000124

Ladd, C., Mordy, C. W., Salo, S. A., & Stabeno, P. J. (2016). Winter water properties and the Chukchi Polynya. *Journal of Geophysical Research: Oceans*, *121*(8), 5516–5534. https://doi.org/10.1002/2016JC011918

Leonard, B. P., MacVean, M. K., & Lock, A. P. (1994). *The flux-integral method for multi-dimensional convection and diffusion, NASA Tech. Memo, 106679/ICOMP-94-13*. Washington, DC: NASA.

Maykut, G. A. (1978). Energy exchange over young sea ice in Central Arctic. *Journal of Geophysical Research*, *83*(C7), 3646–3658. https://doi.org/10.1029/JC083iC07p03646

McLaughlin, F. A., Carmack, E. C., Macdonald, R. W., Melling, H., Swift, J. H., Wheeler, P. A., et al. (2004). The joint roles of Pacific and Atlantic-origin waters in the Canada Basin, 1997–1998. *Deep-Sea Research, Part I*, *51*(1), 107–128. https://doi.org/10.1016/j.dsr.2003.09.010

Melling, H., Haas, C., & Brossier, E. (2015). Invisible polynyas: Modulation of fast ice thickness by ocean heat flux on the Canadian polar shelf. *Journal of Geophysical Research: Oceans*, *120*, 777–795. https://doi.org/10.1002/2014JC010404

Mizobata, K., Watanabe, E., & Kimura, N. (2016). Wintertime variability of the Beaufort Gyre in the Arctic Ocean derived from CryoSat-2/SIRAL observations. *Journal of Geophysical Research: Oceans*, *121*, 1685–1699. https://doi.org/10.1002/2015JC011218

Morales Maqueda, M. A., Willmott, A. J., & Biggs, N. R. T. (2004). Polynya dynamics: A review of observations and modeling. *Reviews of Geophysics*, *42*, RG1004. https://doi.org/10.1029/2002RG000116

Nikolopoulos, A., Pickart, R. S., Fratantoni, P. S., Shimada, K., Torres, D. J., & Jones, E. P. (2009). The western Arctic boundary current at 152°W: Structure, variability, and transport. *Deep-Sea Research, Part II*, *56*(17), 1164–1181. https://doi.org/10.1016/j.dsr2.2008.10.014

Nishino, S. (2013). R/V Mirai Cruise Report MR13–06. JAMSTEC, Yokosuka, Japan. Retrieved from www.godac.jamstec.go.jp/darwin/datatree/e, (last access: 25 September 2017).

Noh, Y., & Kim, H. J. (1999). Simulations of temperature and turbulence structure of the oceanic boundary layer with the improved near-surface processes. *Journal of Geophysical Research*, *104*(C7), 15,621–15,634. https://doi.org/10.1029/1999JC900068

Pickart, R. S., Weingartner, T. J., Pratt, L. J., Zimmermann, S., & Torres, D. J. (2005). Flow of winter-transformed Pacific water into the western Arctic. *Deep-Sea Research, Part II*, *52*(24-26), 3175–3198. https://doi.org/10.1016/j.dsr2.2005.10.009

Rudels, B., Anderson, L. G., & Jones, E. P. (1996). Formation and evolution of the surface mixed layer and halocline of the Arctic Ocean. *Journal of Geophysical Research*, *101*(C4), 8807–8821. https://doi.org/10.1029/96JC00143

Saha, S., Moorthi, S., Pan, H. L., Wu, X., Wang, J., Nadiga, S., et al. (2010). The NCEP climate forecast system reanalysis. *Bulletin of the American Meteorological Society*, *91*(8), 1015–1058. https://doi.org/10.1175/2010BAMS3001.1

Shimada, K., Itoh, M., Nishino, S., McLaughlin, F., Carmack, E., & Proshutinsky, A. (2005). Halocline structure in the Canada Basin of the Arctic Ocean. *Geophysical Research Letters*, *32*, L03605. https://doi.org/10.1029/2004GL021358

Tamura, T., & Ohshima, K. I. (2011). Mapping of sea ice production in the Arctic coastal polynyas. *Journal of Geophysical Research*, *116*, C07030. https://doi.org/10.1029/2010JC006586

Watanabe, E., Onodera, J., Harada, N., Aita, M. N., Ishida, A., & Kishi, M. J. (2015). Wind-driven interannual variability of sea ice algal production in the western Arctic Chukchi Borderland. *Biogeosciences*, *12*(20), 6147–6168. https://doi.org/10.5194/bg-12-6147-2015

Watanabe, E., Onodera, J., Harada, N., Honda, M. C., Kimoto, K., Kikuchi, T., et al. (2014). Enhanced role of eddies in the Arctic marine biological pump. *Nature Communications*, *5*(1), 3950. https://doi.org/10.1038/ncomms4950

Watanabe, E., Onodera, J., Itoh, M., Nishino, S., & Kikuchi, T. (2017). Winter transport of subsurface warm water toward the Arctic Chukchi Borderland. *Deep-Sea Research, Part I*. https://doi.org/10.1016/j.dsr. 2017.08.009

Weingartner, T. J., Aagaard, K., Woodgate, R. A., Danielson, S., Sasaki, Y., & Cavalieri, D. J. (2005). Circulation on the north central Chukchi Sea shelf. *Deep-Sea Research, Part II*, *52*(24-26), 3150–3174. https://doi.org/10.1016/j.dsr2.2005.10.015

Weingartner, T. J., Cavalieri, D. J., Aagaard, K., & Sasaki, Y. (1998). Circulation, dense water formation, and outflow on the northeast Chukchi shelf. *Journal of Geophysical Research*, *103*(C4), 7647–7661. https://doi.org/10.1029/98JC00374

Weingartner, T. J., Potter, R. A., Stoudt, C. A., Dobbins, E. L., Statscewich, H., Winsor, P. R., et al. (2017). Transport and thermohaline variability in Barrow Canyon on the northeastern Chukchi Sea shelf. *Journal of Geophysical Research: Oceans*, *122*, 3565–3585. https://doi.org/10.1002/2016JC012636

Winsor, P., & Björk, G. (2000). Polynya activity in the Arctic Ocean from 1958 to 1997. *Journal of Geophysical Research*, *105*(C4), 8789–8803. https://doi.org/10.1029/1999JC900305

Winsor, P., & Chapman, D. C. (2002). Distribution and interannual variability of dense water production from coastal polynyas on the Chukchi shelf. *Journal of Geophysical Research*, *107*(C7), 3079. https://doi.org/10.1029/2001JC000984

Woodgate, R. A., & Weingartner, T. J. (2015a). Temperature, salinity, velocity including ADCP ice tracking, and bottom pressure collected by Bering Strait Moorings A2W, A2, A4W, A4, A3 from 2010-08-03 to 2011-07-14 (NCEI Accession 0138583). Version 1.1. NOAA National Centers for Environmental Information. Dataset. [24 November 2016].

Woodgate, R. A., & Weingartner, T. J. (2015b). Temperature, salinity, velocity including ADCP ice tracking, and bottom pressure collected from moored buoys in Bering Strait from 2011-07-14 to 2013-07-05 (NCEI Accession 0138173). Version 1.1. NOAA National Centers for Environmental Information. Dataset. [22 November 2016].

Woodgate, R. A., Aagaard, K., Swift, J. H., Falkner, K. K., & Smethie, W. M. Jr. (2005). Pacific ventilation of the Arctic Ocean's lower halocline by upwelling and diapycnal mixing over the continental margin. *Geophysical Research Letters*, *32*, L18609. https://doi.org/10.1029/2005GL023999

Woodgate, R. A., Aagaard, K., Swift, J. H., Smethie, W. M., & Falkner, K. K. (2002). *Chukchi Borderland Cruise CBL2002 Arctic West—Phase II (AWS-02-II)* (p. 51). Seattle, WA: University of Washington. Retrieved from http://psc.apl.washington.edu/CBL.html

Woodgate, R. A., Aagaard, K., & Weingartner, T. J. (2005). A year in the physical oceanography of the Chukchi Sea: Moored measurements from autumn 1990–1991. *Deep-Sea Research, Part II*, *52*(24-26), 3116–3149. https://doi.org/10.1016/j.dsr2.2005.10.016